



An investigation on grinding mechanism of alumina ceramic using a grooved grinding wheel with inclined cross section

C. Li¹ · Z. J. Shi¹ · X. H. Zhang^{1,2} · Z. Y. Shi² · S. Li¹ · R. Y. Jiang¹ · Z. R. Wang¹ · Z. C. Zhang¹

Received: 5 July 2020 / Accepted: 13 October 2020 / Published online: 27 October 2020
© Springer-Verlag London Ltd., part of Springer Nature 2020

Abstract

In this study, a type of the grooved grinding wheel with inclined cross section is designed based on trapezoidal beam. The grinding type of grooved grinding wheel with inclined cross section is used as a new structuring method to process alumina ceramic. The inclined cross-section groove of a grinding wheel can improve the wear-resistant properties of laser macro-structured grinding wheel. First, a pulse laser was used to ablate rectangular cross-section groove and inclined cross-section groove on two bronze-bonded diamond wheels. Second, a grinding test was performed by using the grooved grinding wheel with rectangular cross-section and grooved grinding wheel with inclined cross section. The experimental results showed that the grooved grinding wheel with inclined cross section presented a reduction of grinding forces between 18 and 31.7%, but the better surface was not obtained. In addition, the inclined cross-section groove could reduce stress concentration, thus improving the wear of the grinding wheel surface. This indicates that the grooved grinding wheel with inclined cross section has better grinding performance than the grooved grinding wheel with rectangular cross section owing to the inclined cross-section structures. This provides further evidence for a method of constructing grooved grinding wheel with inclined cross section based on trapezoidal beam design.

Keywords Inclined cross section · Grinding force · Surface roughness · Wear

1 Introduction

As an advanced engineering ceramic, alumina ceramic is widely used in aerospace, medical fields, and other important industrial fields, which has high mechanical strength and high temperature resistance [1–3]. However, alumina ceramic is more difficult to process and has high machining and finishing costs because of their high hardness and high strength. The demand of high accuracy alumina ceramic is increasing with the development of technology [4, 5]. Conventional grinding techniques can no longer meet the requirements of precision manufacturing community. Therefore, the study of machining

technique during the machining is important for improving the accuracy of alumina ceramic.

Laser structure technology has obvious advantages in machining advanced materials compared with the conventional grinding technology [6–10]. First of all, Walter et al. [11] proposed a novel laser method for CBN grinding wheel based on surface structuring with ultrashort picosecond pulsed lasers. Although the grinding force could be reduced between 25 and 54%, the wear rate of the structured tools was higher than the non-structural tools. Then, to improve the surface quality of the workpiece, Deng et al. [12] studied the influence of the micro-structure pattern on the performance of laser micro-structured coarse-grained diamond grinding wheels. The results of the experiments showed that better workpiece surface quality was obtained when using micro-structured grinding wheel. However, the wear resistance of micro-structured grinding wheel was obviously lower than that of non-structured grinding wheel. The above-mentioned investigations indicate that the grinding force and surface roughness of the workpiece can be reduced by using the micro-structured grinding wheel. Nevertheless, the coolant transportation ability and the lubrication capability are not obvious. In order to improve the coolant

✉ Z. J. Shi
szj15057171806@163.com

¹ College of Mechanical Engineering, Hunan Institute of Science and Technology, Yueyang 414006, People's Republic of China

² Beijing Engineering Research Center of Precision Measurement Technology and Instruments, Beijing University of Technology, 100 Ping Le Yuan, Chaoyang District, Beijing 100124, China

transportation ability and the lubrication capability of grinding, Zhang et al. [13, 14] put forward laser macro-structured grinding wheel (LMSG). The grooves were contributed to chip disposal and coolant flow, thereby reducing the effect of chip and the grinding temperature. However, the wear of grinding wheel was serious on the macroscopic level near the groove edge. From the literature review above, the research objects are mainly grooved grinding wheel with rectangular cross section, and the primary reason for the short life of laser macro-structured grinding wheel is the insufficient structural strength. In order to improve wear-resistant properties of laser macro-structured grinding wheel, we put forward grooved grinding wheel with inclined cross section (ICSG). In accordance with the findings in the literature, the inclined cross-section technology had been used in thermal sciences and engineering structures. For example, trapezoidal structure had prominent advantages over rectangular structure enhancement in heat transfer [15, 16]. The trapezoidal structure increased both ductility and the ultimate load-carrying capacity of the beams [17]. Therefore, it can be assumed that inclined cross-section groove can improve the coolant ability and wear-resistant properties of laser macro-structured grinding wheel.

In this paper, we introduced a grooved grinding wheel with inclined cross section inspired by the structure of the trapezoidal beam. The inclined-cross-section groove and rectangular-cross-section groove were introduced as the grinding parameter for discussing the better groove structure. First, the method for manufacturing the grooved grinding wheel with rectangular cross section and grooved grinding wheel with inclined cross section was developed. Subsequently, alumina ceramics were ground using the grooved grinding wheel with rectangular cross section and grooved grinding wheel with inclined cross section. The grinding forces and the surface quality of the workpieces as well as the wear of grinding wheels were comparatively analyzed.

2 Experimental details

2.1 Experimental apparatus and materials

The bronze-bonded diamond grinding wheels are manufactured using a compact pulsed ytterbium-doped fiber laser (model: YCP-1-120-50-50-HC-RG). The workpiece is alumina ceramic with the dimension of $30 \times 30 \times 10$ mm. The laser apparatus is displayed in Fig. 1. The schematic diagram of the structuring method is depicted in Fig. 2. The details of the grinding wheels are tabulated in the Table 1. The mechanical properties of the workpiece are listed in Table 2.

The grinding experiments are carried out in the down-grinding mode on the precision plane grinder (model MUGK7120×5) to evaluate the grinding performance of the

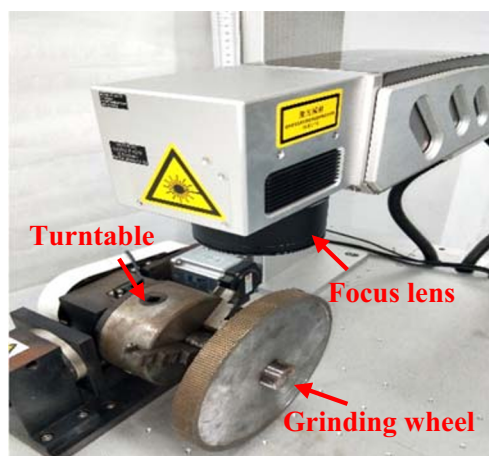


Fig. 1 Experimental apparatus for laser structured

grooved grinding wheel with rectangular cross section and grooved grinding wheel with inclined cross section. The coolant is a 3% solution of water-based coolant, and the flow rate of cooling fluid is 18 L/min in all the experiments. In the experiment, the normal and tangential grinding forces are monitored with a high-accuracy dynamometer (Kistler 9256C2). After each set of experiments, the surface roughness of the workpieces is measured with a contact probe profilometer. The 3D optical microscope with an ultra-deep depth of field is used to evaluate the ground surface morphology of the workpieces and the wear of grinding wheels. The experimental device for grinding is shown in Fig. 3. The grinding parameters are listed in Table 3.

2.2 Design of inclined cross-section groove

Based on the above, the cross section of inclined cross-section groove is shown in Fig. 4, where y is the direction of the tangential force, z is the direction of the normal force, h is the height, and the hems of the trapezoid are u and l , respectively.

Therefore, the section inertia moment I_y of Y-axis is given by

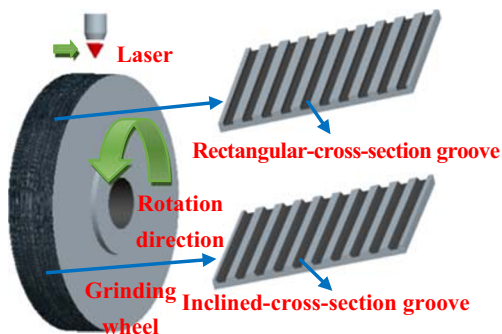


Fig. 2 Schematic view of laser macro-structuring

Table 1 The specifications of bronze-bonded diamond grinding wheel

| | |
|------------------------------|-------------|
| Wheel type | SDC120N100B |
| Wheel diameter (mm) | 200 |
| Bore diameter (mm) | 32 |
| Wheel width (mm) | 20 |
| Depth of abrasive layer (mm) | 5 |
| Grain size (μm) | 70~130 |
| Concentration | 75% |
| Abrasive material | Diamond |

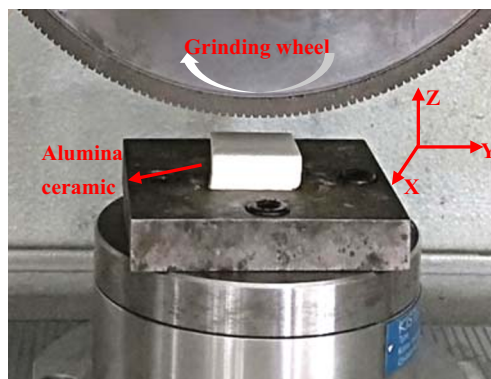


Fig. 3 Experimental apparatus for grinding alumina ceramic

$$I_y = \frac{h^3}{36(u+l)} (u^2 + 4ul + l^2) \tag{1}$$

and the section inertia moment I_z of Z-axis is given by

$$I_z = \frac{1}{48} h(u+l)(u^2 + l^2) \tag{2}$$

Using Eqs. (1) and (2),

$$f = \frac{I_y}{I_z} = \frac{4h^2(u^2 + 4ul + l^2)}{3(u+l)^2(u^2 + l^2)} = \frac{4}{3} \left(\frac{h}{l}\right)^2 \frac{1 + 4\varphi + \varphi^2}{(1 + \varphi)^2(1 + \varphi^2)} \tag{3}$$

where $\varphi = \frac{u}{l}$ ($0 \leq \varphi \leq 1$). The partial derivative with respect to φ in Eq. (4) is

$$\frac{\partial}{\partial \varphi} \left(\frac{I_y}{I_z}\right) = -\frac{4}{3} \left(\frac{h}{l}\right)^2 \frac{(\varphi^4 + 6\varphi^3 + 4\varphi^2 + 2\varphi - 1)^2}{(1 + \varphi)^2(1 + \varphi^2)} \tag{4}$$

If $\varphi = 0.6$, then $f = 1.44 \left(\frac{h}{l}\right)^2$.

In this work, in order to improve the wear-resistant properties of the grooved grinding wheel with inclined cross section and retain more effective grains as much as possible, we determine the φ value as 0.6 in comprehensive consideration of the parameter. Meanwhile, $w = l + 0.35u$, $h/l = 0.576$. When $\varphi = 0.6$, the ratio of the Y-axis stiffness to the Z-axis stiffness is 0.478; when $\varphi = 1$, the ratio of the Y-axis stiffness to the Z-axis stiffness is 0.166. It means that the distortion-resistant ability of the grooved grinding wheel with inclined

cross section is approximately 31.2% higher than the distortion-resistant ability of the grooved grinding wheel with rectangular cross section.

2.3 Laser structuring

The sizes of grooved grinding wheel with rectangular cross section and grooved grinding wheel with inclined cross section were designed. Figure 5 showed the laser structuring patterns and their dimensions. The characteristic dimensions of the rectangular cross-section groove were the groove width W , the groove spacing I , and the depth of the groove D . The characteristic dimensions of the inclined-cross-section groove were the groove upper-bottom length U , the groove lower-bottom length L , and the groove spacing S . The depth of the inclined-cross-section groove was consistent with the rectangular-cross-section groove.

Before the laser ablation operations, the grinding wheels were dressed to create equivalent surface conditions for grinding wheel. After that, the grinding wheels were machined precisely by a stable pulsed laser (average power = 20 W, wavelength = 1064 nm, pulse width = 10 ms, pulse frequency = 30 kHz, scanning speed = 2200 mm/s). The laser beam was focused perpendicular to the surface of grinding wheel by an achromatic lens with a focal length of 33 mm. The surface of the grinding wheel was subjected to laser structuring to introduce rectangular-cross-section groove shape. Meanwhile, to reduce the formation of the re-solidified layer, the molten material could be blown away from the grooves with assistant gas [18]. This method could precisely control the groove

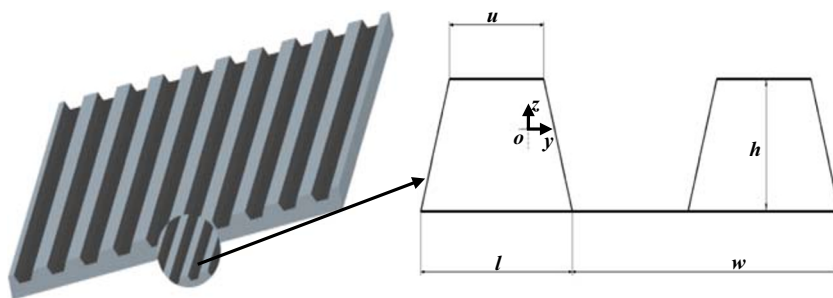
Table 2 Nominal properties of alumina ceramic used

| Ceramic | Density (kg/m ³) | Flexure strength (MPa) | Vickers hardness (GPa) | Fracture toughness (MPa m ^{1/2}) |
|---------|------------------------------|------------------------|------------------------|--|
| Alumina | 3.7×10^3 | 500 | 18.3 | 5.3 |

Table 3 Grinding test parameters

| Category | Content |
|-------------------------------|------------|
| Depth of grinding a_p (μm) | 5 |
| Wheel speed v_s (m/s) | 35 |
| Workpiece speed v_w (m/min) | 2, 4, 6, 8 |

Fig. 4 Cross section of the inclined-cross-section groove



spacing. The groove spacing was set to 2.3 mm. As shown in Fig. 6a, the groove width and the groove depth were identical ($W = 0.65$ mm, $D = 0.95$ mm) for the rectangular grooves. Inclined-cross-section grooves were realized by scanning the surface line with a focused laser beam. The position of the laser beam was from the focal point of the laser beam to 0.95 mm below the focal point of the laser beam. This was done in 8 groups. The width of ablation was 1 mm for the first time, and the width of the next ablation was 0.08 mm smaller than the width of the previous ablation. The depth of each ablated was 0.12 mm. Compared with the rectangular-cross-section groove, the inclined-cross-section groove had larger space. Therefore, to ensure the same number of grooves, the groove spacing of the inclined-cross-section grooves was reduced. The groove spacing was set to 2 mm. As shown in Fig. 6b, the groove upper bottom length, the groove lower bottom length, and the depth of the groove were identical ($U = 1$ mm, $L = 0.35$ mm, $D = 0.95$ mm) for the inclined-cross-section grooves.

3 Results and discussion

3.1 Grinding forces

Figure 7 showed the images of the grinding force of the alumina ceramic using different workpiece speed with a stable wheel speed of 35 m/s and a fixed grinding depth of 5 μ m. As shown in Fig. 7, the use of higher workpiece speed produced a

higher grinding force. The possible reason was increased in radial penetration depth of grains. It resulted the increasing of the grinding force. This was identical to traditional grinding principle [19–21]. It was more important that the normal grinding force F_n , and the tangential grinding force F_t could be effectively reduced in ICSG condition. The contact areas between the inclined-cross-section grooved grinding wheel and workpiece surface were smaller than the contact areas between the rectangular-cross-section grooved grinding wheel and workpiece surface, so the number of abrasive grains in contact with the workpiece surface was reduced. Therefore, less energy was used to offset the sliding and friction resistance. It could also be seen from Fig. 6 that the grooved grinding wheel with inclined-cross-section could provide larger space for chip. This reduced the effect of chip on the grinding force.

3.2 Surface roughness and surface morphology

3.2.1 Surface roughness

The roughness of the workpiece R_a was measured at sampling length of 0.8 mm and evaluation length of 4 mm. Figure 8 illustrates the images of the surface roughness of alumina ceramic. The use of lower workpiece speed produced better workpiece surface quality, because the residual area height was reduced by the lower workpiece speed. However, it was also seen in Fig. 8 that the surface roughness of alumina ceramic became rougher after grinding by ICSG condition. The

Fig. 5 Overview of produced patterns and their dimensions. **a** LMSG. **b** ICSG

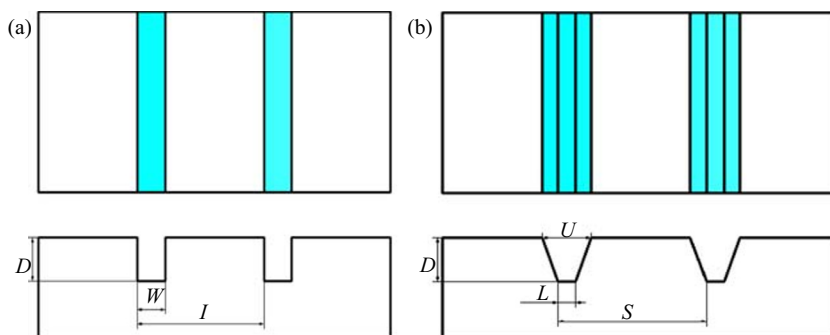
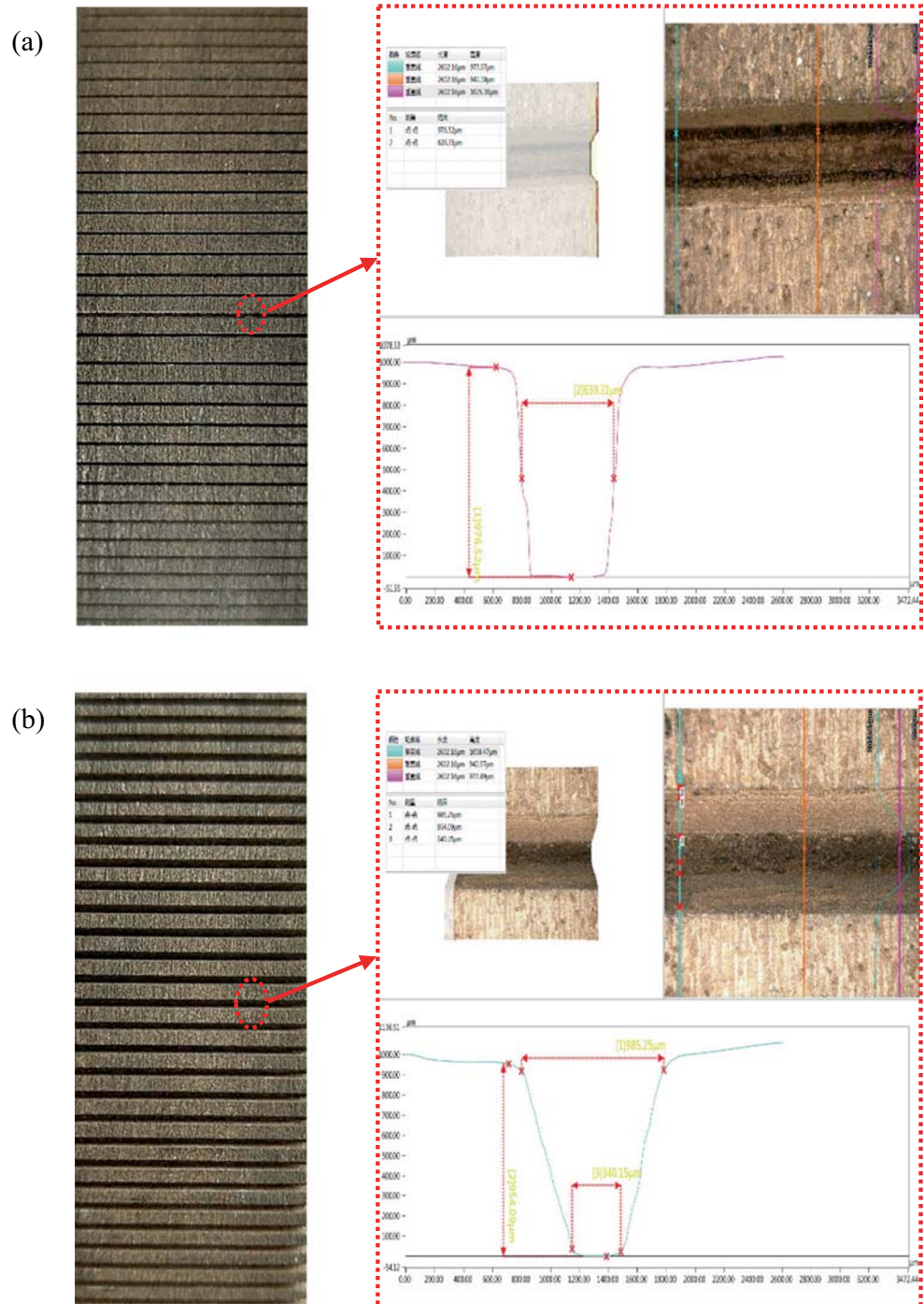


Fig. 6 Optical microscope images of laser-structured grinding wheels. **a** LMSG. **b** ICSG



ICSG grinding type had a smaller contact area than the LMSG grinding type. This resulted in a reduction in the number of active cutting edges that could improve the surface quality of workpiece. However, the pressure of a single abrasive particle is reduced because of the structural characteristics of the inclined cross-section groove. From previous research, it was known that lower forces normally lead to a higher roughness of the workpiece surface [22]. Therefore, it could be observed

from Fig. 8 that the surface roughness of alumina ceramic became rougher after grinding by ICSG condition.

3.2.2 Surface morphology

The morphologies of the workpieces surface were examined at $\times 500$ and $\times 1000$ magnifications. Figure 9 showed the morphology of alumina ceramic under the same workpiece

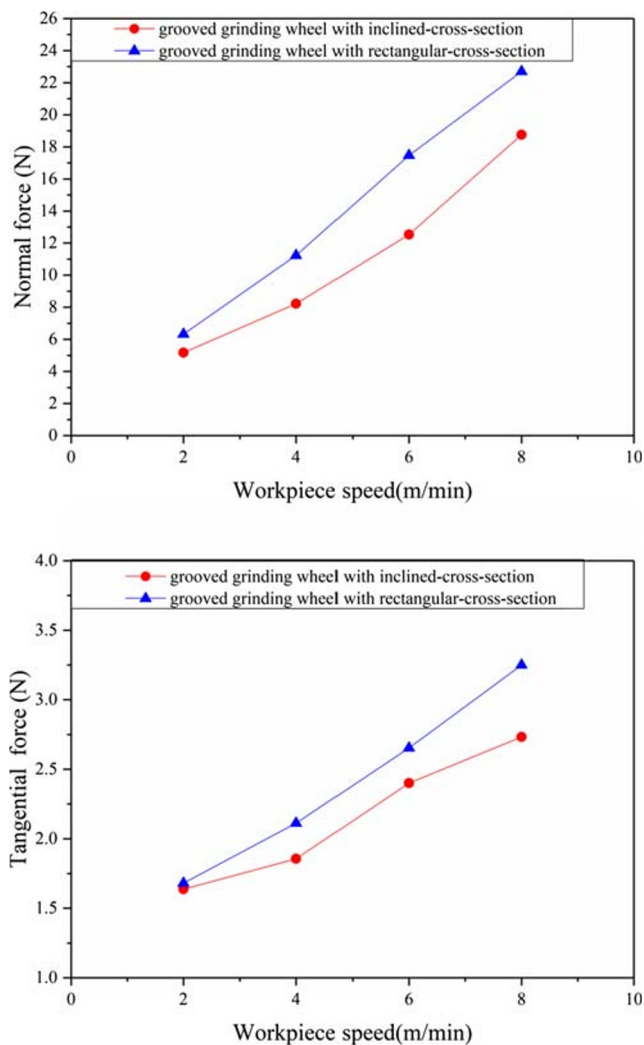


Fig. 7 The relationship between grinding forces and workpiece speed

speed of 4 m/min. As illustrated in Fig. 9, some smooth areas could be observed on all the workpiece surfaces. This could be

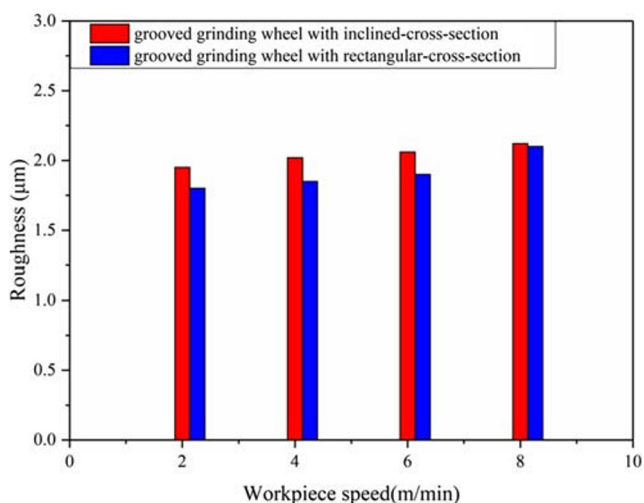


Fig. 8 Effect of the workpiece speed on surface roughness

interpreted that plastic flow was more suitable for material removal than brittle fracture when the dimensional scale of material removal was small enough. However, it was clear that the surface quality had worsened when using grooved grinding wheel with inclined cross-section. It could be summarized that the chip thickness became relatively higher when the contact layer was decreased. In this condition, the main workpiece removal way was cutting action rather than plowing. Therefore, it could be observed from Fig. 9b that the texture of the workpiece surface scratches became rougher. Besides, some cracks were observed, especially around the pits. This result could be interpreted as follows: the undeformed thickness under the ICSG condition was larger than the undeformed thickness under the LMSG condition. The larger undeformed thickness led to an increase in the number of brittle cracks. Then, the emergence of brittle cracks produced more irregular pits [23].

3.3 Wear of grinding wheels

The first area to be observed was the groove surface after grinding. As seen from Fig. 10, some grains had been pulled out on the groove edge. This may be the abrasive grains at the edge of the grooves were subjected to larger contact pressures. Furthermore, both the grooved grinding wheel with inclined cross section and grooved grinding wheel with rectangular cross section had edge wear. In the grinding process, grinding force was transmitted from the abrasive grain apexes to the edge of the groove. Then, fatigue cracks at the edge of the groove under the action of repeated stress loading were produced. Eventually, the wear of groove edge was formed due to interference between adjacent fatigue cracks. More importantly, the wear of groove edge could be reduced effectually owing to the structure of inclined cross-section groove. In the grinding type of the grooved grinding wheel with inclined cross section, the inclined-cross-section groove could reduce stress concentration. This would contribute to enhancing the stability of the groove structure. Interestingly, the groove edge displayed a sign that the groove edge would turn into a smooth rounded corner, especially on the groove edge of grooved grinding wheel with rectangular cross section. This finding suggests that smooth rounded groove edge structure may further reduce the wear of groove edge.

The second area to be observed was the non-structured surface. It was evident from Fig. 11 that some grains had been pulled out and left a cavity on the grinding wheel surface. The main reason was that grains lack mechanical anchorage. Moreover, it was also seen in Fig. 11 that some grains had been fractured on the grinding wheel. On the one hand, grinding force increased rapidly when the workpiece started to contact the grains. This could have resulted in the fracture of grains. On the other hand, under the influence of strain and temperature, cracks were generated on the surface of the

Fig. 9 Ground surface morphology of alumina ceramic under **a** LMSG and **b** ICSG condition

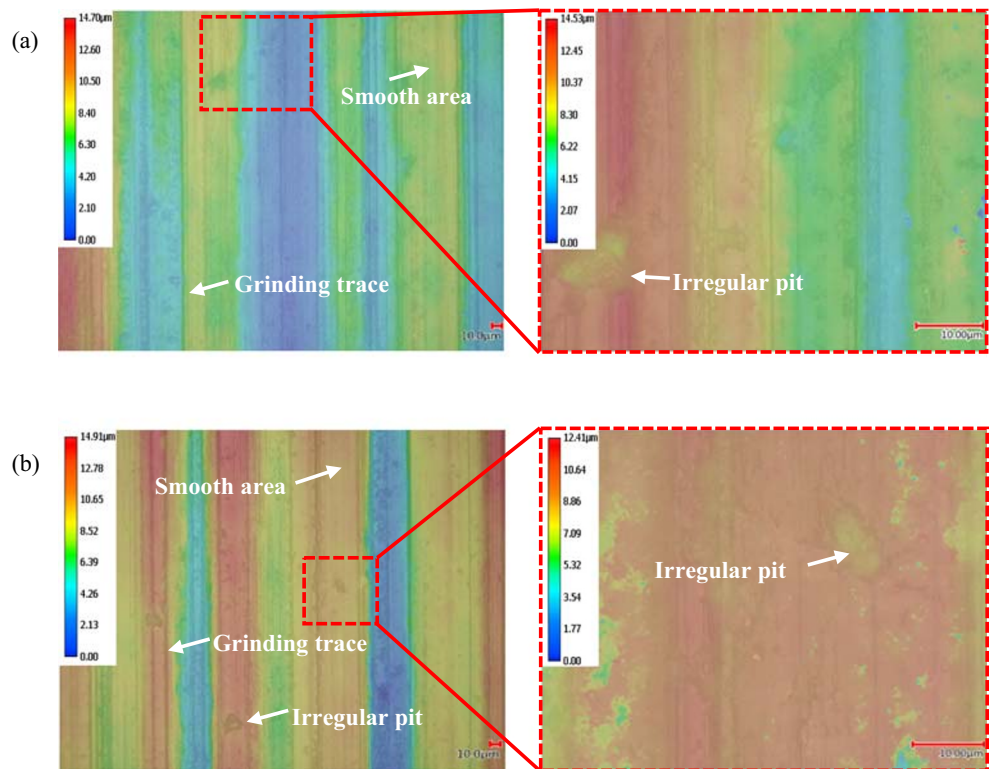
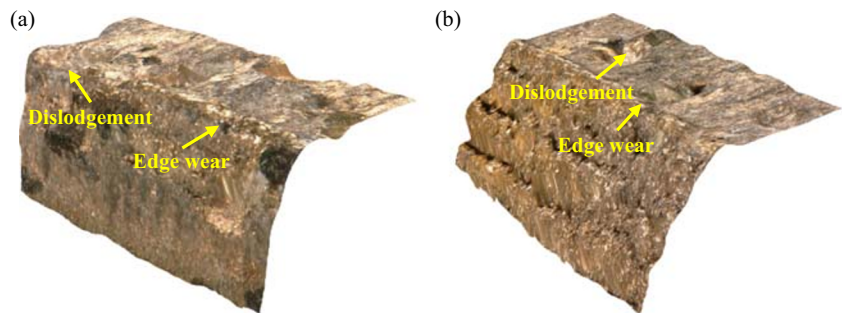


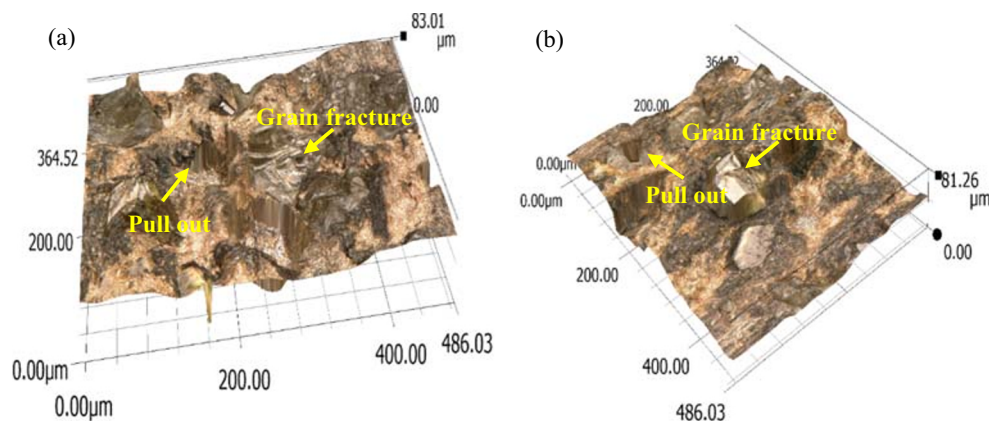
Fig. 10 Micrographs of groove edge by **a** LMSG and **b** ICSG



abrasive grains. These cracks under the repeated action of grinding forces were extended and broken. Finally, some grains had been fractured. It is important to note that the

new cracks of grains still extend even when the grain is no longer in contact with the workpiece [24]. It can be seen that abrasive fractures can be effectively decreased by reducing the

Fig. 11 Micrographs of grits after **a** LMSG and **b** ICSG



initiation of abrasive surface cracks. Under ICSG grinding type, the surface stress of the grinding wheel was relatively low, thus reducing the stress of single abrasive grain. This would greatly reduce the fracture probability of abrasive particles. Therefore, the degree of grains fracture was remarkably reduced when using the grooved grinding wheel with inclined cross section, as shown in Fig. 11b. However, the abrasive wear will adversely affect the grinding process [25–29]. For example, Ding et al. [30] studied the effect of grains wear on silicon carbide by ultrasonic vibration-assisted grinding. The results indicated that grain wear affect the workpiece surface quality significantly. Grains wear became more serious with increasing grinding passes. The grains cannot effectively participate in grinding, and more scratching occurred. Consequently, it can be seen that grooved grinding wheel with inclined cross section is more practical than grooved grinding wheel with rectangular cross section, especially in the later stage of the grinding process.

4 Conclusions

A grooved grinding wheel with inclined cross section was invented for alumina ceramic surface grinding for enhancing the grinding performance. The effect of two processing patterns on the grinding force and workpiece quality was investigated. Moreover, the wear of the grooved grinding wheel with rectangular cross section and grooved grinding wheel with inclined cross section was comparatively evaluated. Based on the experimental results, the following conclusions can be drawn: Compared with the grooved grinding wheel with rectangular cross section, the grooved grinding wheel with inclined cross section shows a reduction of grinding forces between 18 and 31.7%. However, the roughness of the workpiece R_a is not clearly improved. The roughness of the workpiece that is ground by the grooved grinding wheel with inclined cross section is 8% more than that of the workpiece ground by grooved grinding wheel with rectangular cross section. What is more important, the wear-resistant properties of laser macro-structured wheel have significant improvement because of the structural characteristics of the inclined cross-section groove. For the grooved grinding wheel with inclined cross section, the groove structure can be further optimized. In future study work, the smooth rounded corner of groove edge and the angle of the inclined cross-section groove may be studied, mainly to improve the grinding performance of grooved grinding wheel with inclined cross section.

Funding This project was sponsored by the National Natural Science Foundation of China (grant no. 51875200), the National Key R&D Program of China (grant no. 2018YFB2001400), and the Science and Technology Planning Project of Hunan Province (grant no. 2018RS3100) and the Graduate Innovation Foundation of Hunan Province (grant no. CX20190916).

References

1. Tanaka Y, Takakura Y, Kadono K, Taniguchi A, Hayashi K, Iida J, Sugimoto KI, Tohma Y, Ohgushi H (2003) Alumina ceramic talar body prosthesis for idiopathic aseptic necrosis of the talus. *Key Eng Mater* 240-242:805–808
2. Taniguchi A, Takakura Y, Tanaka Y, Kurokawa H, Tomiwa K, Matsuda T, Kumai T, Sugimoto K (2015) An alumina ceramic total talar prosthesis for osteonecrosis of the talus. *J Bone Joint Surg Am* 97(16):1348–1353
3. Lu XW, Yang JN, Li XY, Sun FY, Wang F, Chao YQ (2019) Effects of phase transformation on properties of alumina ceramic membrane: a new assessment based on quantitative X-ray diffraction (QXRD). *Chem Eng Sci* 199:349–358
4. Mohammed MK, Umer U, Al-Ahmari A (2016) Optimization of laser micro milling of alumina ceramic using radial basis functions and MOGA-II. *Int J Adv Manuf Technol* 91(5-8):2017–2029
5. Zou YH, Xie HJ, Dong CW, Wu JZ (2018) Study on complex micro surface finishing of alumina ceramic by the magnetic abrasive finishing process using alternating magnetic field. *Int J Adv Manuf Technol* 97(5-8):2193–2202
6. Deng H, He J (2017) A study of the grinding performance of laser micro-structured coarse-grained diamond grinding wheels. *Int J Adv Manuf Technol* 93(5-8):1989–1997
7. Guo B, Wu MT, Zhao QL, Liu H, Zhang J (2018) Improvement of precision grinding performance of CVD diamond wheels by micro-structured surfaces. *Ceram Int* 44(14):17333–17339
8. Guo B, Zhao QL, Fang XY (2014) Precision grinding of optical glass with laser micro-structured coarse-grained diamond wheels. *J Mater Process Technol* 214(5):1045–1051
9. Zhang XH, Wen DD, Shi ZY, Li S, Kang ZX, Jiang J, Zhang ZC (2020) Grinding performance improvement of laser micro-structured silicon nitride ceramics by laser macro-structured diamond wheels. *Ceram Int* 46(1):795–802
10. Zhang XH, Kang ZX, Li S, Shi ZY, Wen DD, Jiang J, Zhang ZC (2019) Grinding force modelling for ductile-brittle transition in laser macro-micro-structured grinding of zirconia ceramics. *Ceram Int* 45(15):18487–18500
11. Walter C, Komischke T, Kuster F, Wegener K (2014) Laser-structured grinding tools – generation of prototype patterns and performance evaluation. *J Mater Process Technol* 214(4):951–961
12. Deng H, Xu Z (2019) Dressing methods of superabrasive grinding wheels: a review. *Int J Adv Manuf Technol* 45:46–69
13. Zhang XH, Kang ZX, Li S, Wu QP, Zhang ZC (2018) Experimental investigations on the impact of different laser macro-structured diamond grinding wheels on alumina ceramic. *Int J Adv Manuf Technol* 96(5-8):1959–1969
14. Zhang XH, Zhang ZC, Deng ZH, Li S, Wu QP, Kang ZX (2019) Precision grinding of silicon nitride ceramic with laser macro-structured diamond wheels. *Opt Laser Technol* 109:418–428
15. Kumar P (2019) Numerical investigation of fluid flow and heat transfer in trapezoidal microchannel with groove structure. *Int J Therm Sci* 136:33–43
16. Bilen K, Cetin M, Gul H, Balta T (2009) The investigation of groove geometry effect on heat transfer for internally grooved tubes. *Appl Therm Eng* 29(4):753–761
17. Ha GJ, Kim YY, Cho CG (2008) Groove and embedding techniques using CFRP trapezoidal bars for strengthening of concrete structures. *Eng Struct* 30(4):1067–1078
18. Mao C, Sun XL, Huang H, Kang CW, Zhang MJ, Wu YQ (2016) Characteristics and removal mechanism in laser cut-ting of cBN–WC–10Co composites. *J Mater Process Technol* 230:42–49
19. Liu W, Deng ZH, Shang YY, Wan LL (2017) Effects of grinding parameters on surface quality in silicon nitride grinding. *Ceram Int* 43(1):1571–1577

20. Yao CF, Wang T, Xiao W, Huang XC, Ren JX (2014) Experimental study on grinding force and grinding temperature of Aermet 100 steel in surface grinding. *J Mater Process Technol* 214(11):2191–2199
21. Mao C, Liang C, Zhang YC, Zhang MJ, Hu YL, Bi ZM (2017) Grinding characteristics of cBN-WC-10Co composites. *Ceram Int* 43(18):16539–16547
22. Denkena B, Grove T, Götsching T, da Silva EJ, Coelho RT, Filletti R (2014) Enhanced grinding performance by means of patterned grinding wheels. *Int J Adv Manuf Technol* 77(9-12):1935–1941
23. Wan LL, Dai P, Li L, Deng ZH, Hu YX (2019) Investigation on ultra-precision lapping of A-plane and C-plane sapphires. *Ceram Int* 45(9):12106–12112
24. Huang X, Li HN, Rao ZW, Ding WF (2019) Fracture behavior and self-sharpening mechanisms of polycrystalline cubic boron nitride in grinding based on cohesive element method. *Chin J Aeronaut* 32(12):2727–2742
25. Ding WF, Zhu YJ, Xu JH, Su HH (2015) Comparative investigation on brazing behavior, compressive strength, and wear properties of multicrystalline CBN abrasive grains. *Adv Mech Eng* 6:461287–461287
26. Ding WF, Miao Q, Zhu YJ, Xu JH, Fu YC (2014) Comparative investigation on wear behavior and self-sharpening phenomenon of polycrystalline cubic boron nitride and monocrystalline cubic boron nitride grains in high-speed grinding. *Proc IMechE B J Eng Manuf* 230(4):710–721
27. Ding WF, Zhu YJ, Zhang LC, Xu JH, Fu YC, Liu WD, Yang CY (2015) Stress characteristics and fracture wear of brazed CBN grains in monolayer grinding wheels. *Wear* 332-333:800–809
28. Ding WF, Linke B, Zhu YJ, Li Z, Fu YC, Su HH, Xu JH (2017) Review on monolayer CBN superabrasive wheels for grinding metallic materials. *Chin J Aeronaut* 30(1):109–134
29. Deng ZH, Lv LS, Li SC, Wan LL, Liu W, Yan C, Zhang H (2016) Study on the model of high efficiency and low carbon for grinding parameters optimization and its application. *J Clean Prod* 137:1672–1681
30. Ding K, Fu YC, Su HH, Gong XB, Wu KQ (2014) Wear of diamond grinding wheel in ultrasonic vibration-assisted grinding of silicon carbide. *Int J Adv Manuf Technol* 71(9-12):1929–1938

Publisher's note Springer Nature remains neutral with regard to jurisdictional claims in published maps and institutional affiliations.